Supplement of Hydrol. Earth Syst. Sci., 28, 1493–1514, 2024
https://doi.org/10.5194/hess-28-1493-2024-supplement


Hydrology and Earth System Sciences
Open Access
EGU

*Supplement of*

# On the regional-scale variability in flow duration curves in Peninsular India

**Pankaj Dey et al.**

*Correspondence to:* Pankaj Dey (pdey609@gmail.com)

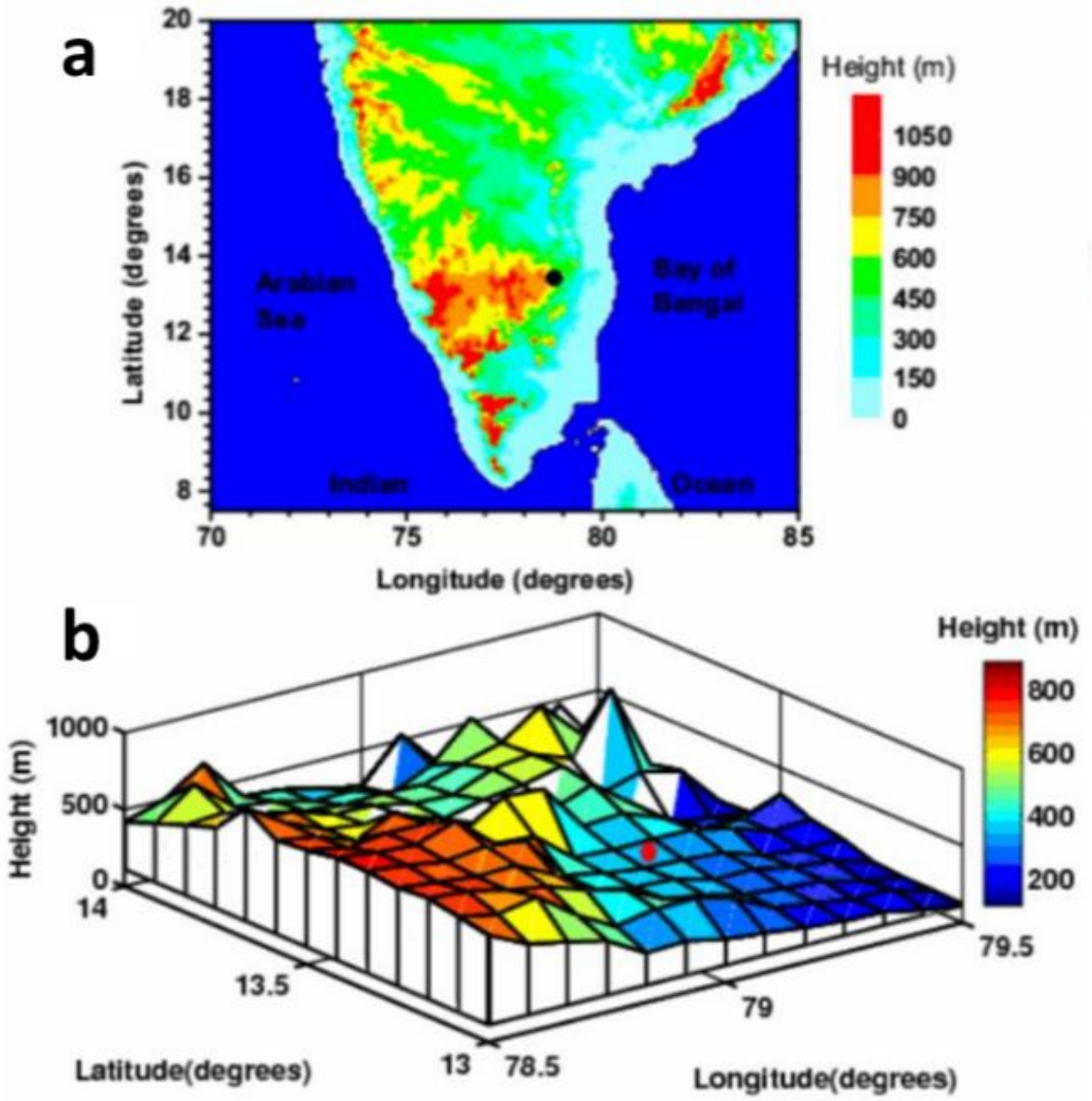


**Figure S1.** (a) Topography map of Peninsular region. The black circle represents the location of Gadanki in the Peninsular system [Reprinted from: (Jayaraman et al., 2010)] (b) High-resolution topography map for 50 km radius around the selected location of Gadanki [Reprinted from: (Jayaraman et al., 2010)].

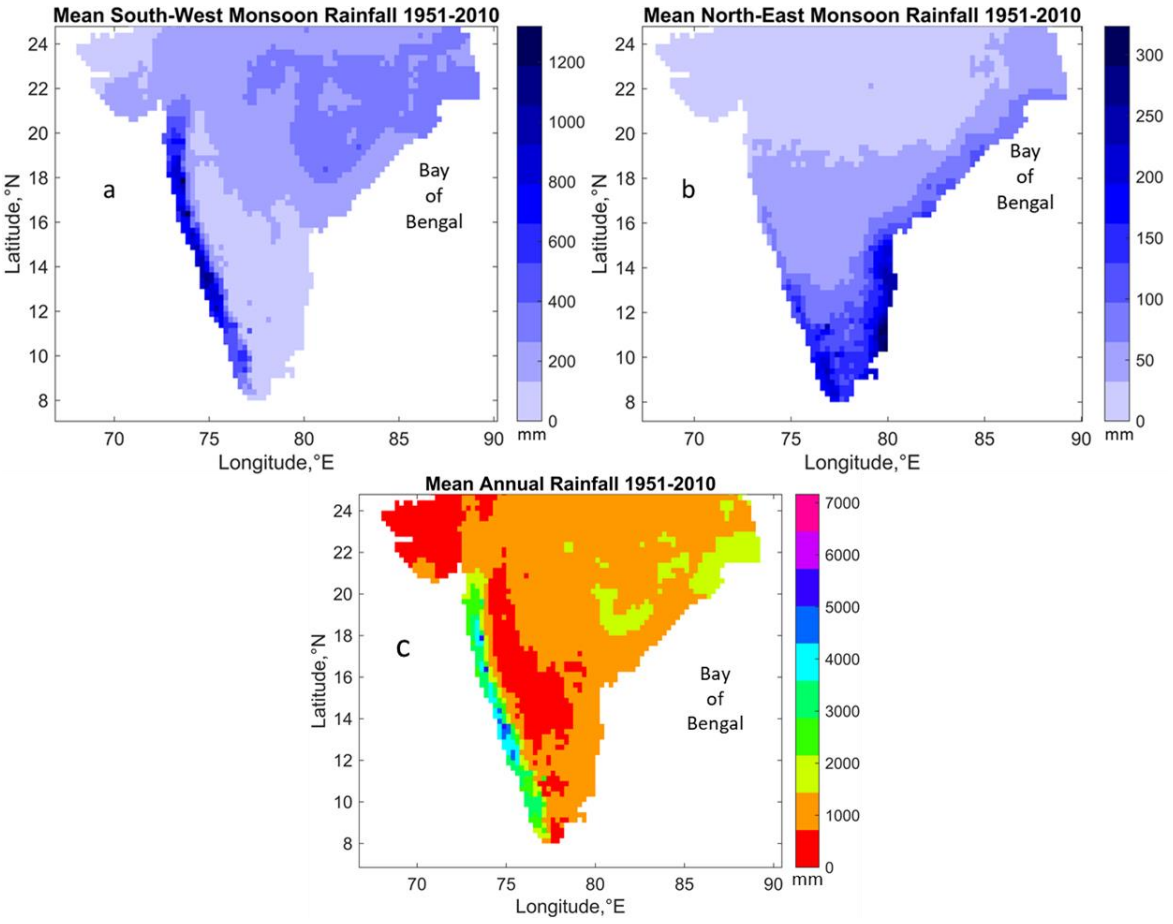


**Figure S2**. Spatial variation of South-West, North-East monsoon and annual rainfall in Peninsular India. The South-West monsoon (a) causes heavy rainfall along the Western Ghats. After crossing the Western Ghats, the rainfall reduces towards north-west direction. The low pressure systems which is caused due to synoptic-scale tropical disturbances formed over Bay of Bengal, moves in north-western direction towards mainland India. This low pressure systems brings significant amount of rainfall over the central India (Krishnamurthy and Ajayamohan, 2010; Prakash et al., 2015). The North-East monsoon (b) rainfall occurs mostly in the southern part of Peninsular region. The influence of both South-West and North-East monsoons introduce a bimodal seasonal patterns in monthly rainfall in the southern part of the Peninsular region.

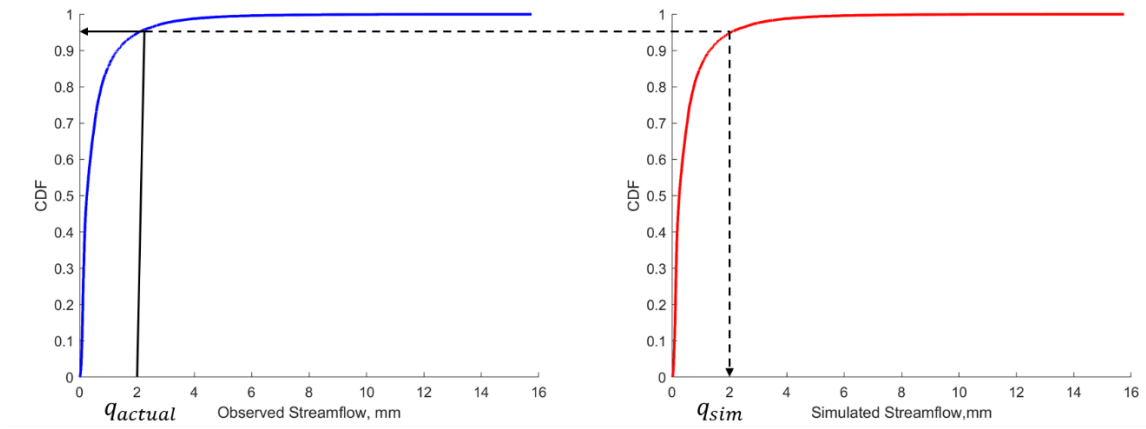


**Figure S3.** Estimation of $q_{\mathrm{sim}}$ using constructed annual CDF. The non-exceedance probability (denoted by CDF – shown in continuous black line) corresponding to actual streamflow ($q_{\mathrm{actual}}$) is used to estimate the $q_{\mathrm{sim}}$ based on the constructed annual CDF (shown in dashed black line). The CDF corresponding to $q_{\mathrm{sim}}$ is developed based on equation 6.

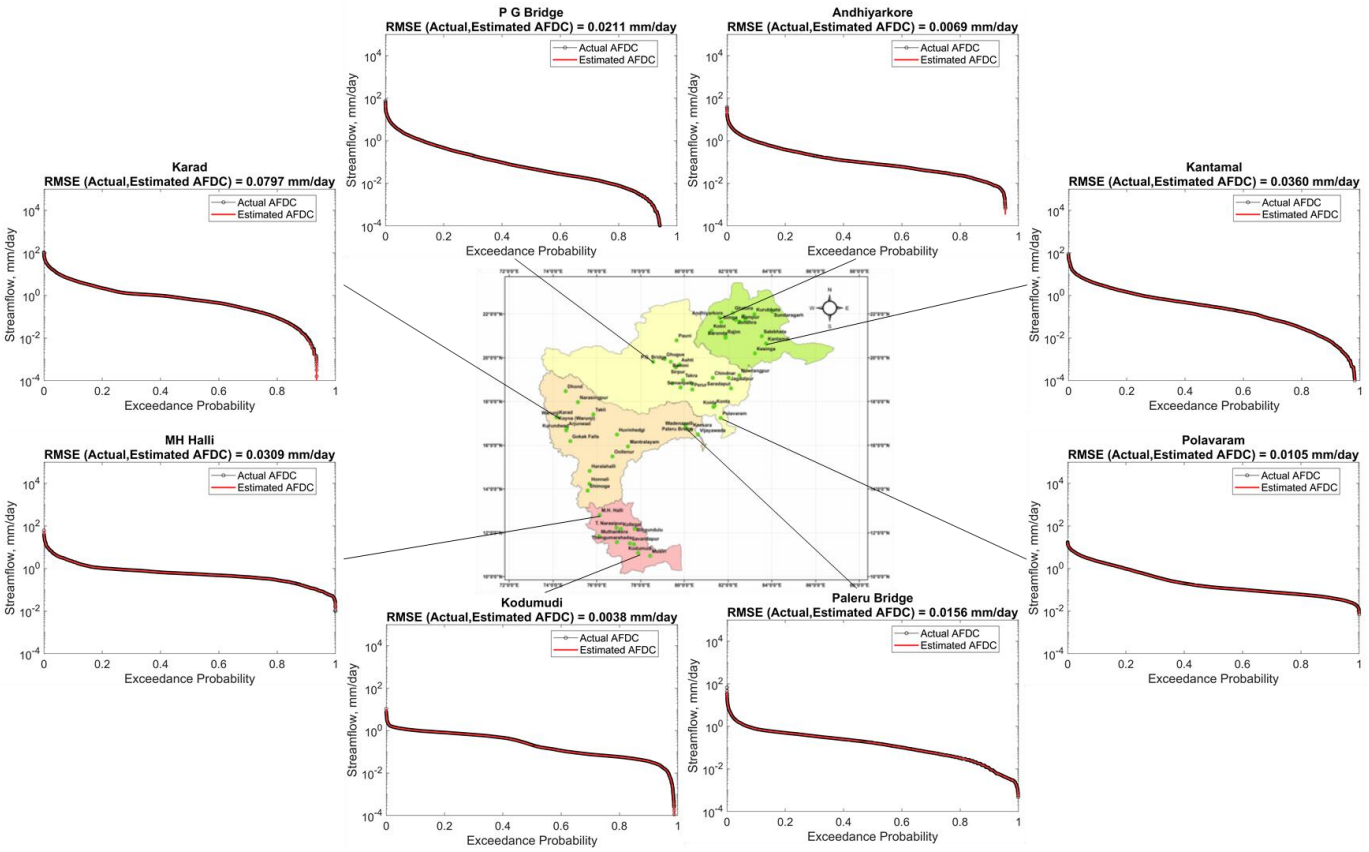


**Figure S4**. Performance of time scale partitioning framework for monthly flows in approximating the annual flow duration curve.

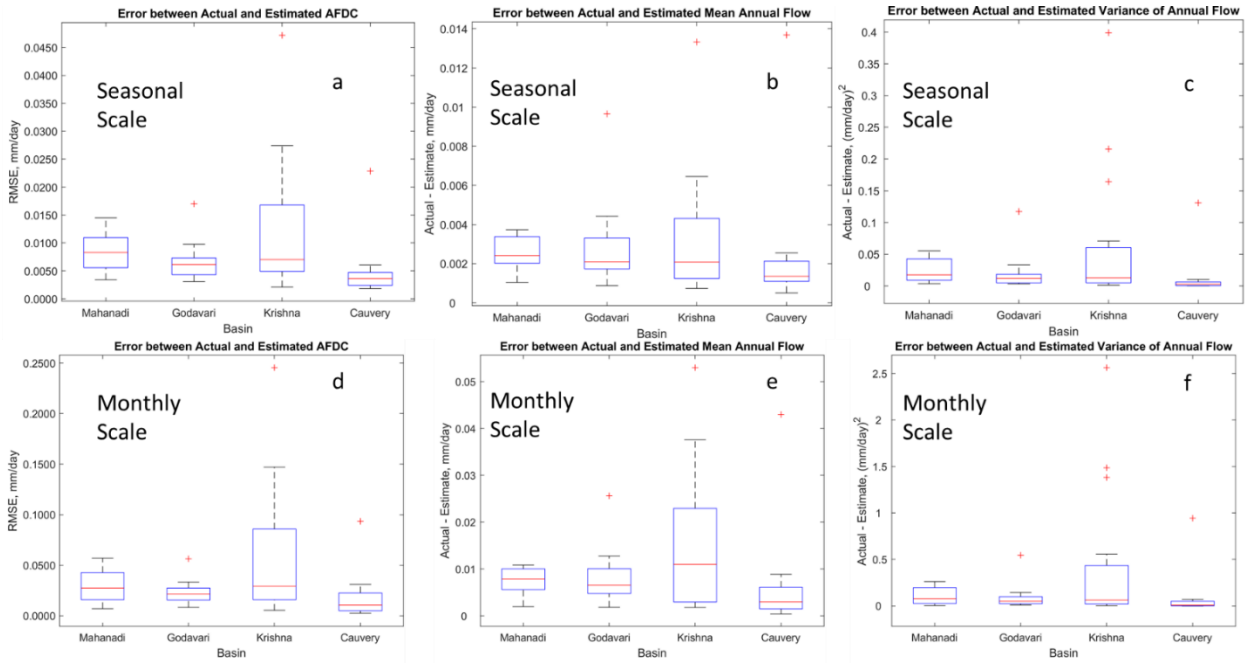


**Figure S5**. Performance of seasonal and monthly time scale partitioning of streamflow in approximating annual flow duration curve (a and d) and estimation of mean (b and e) and variance (c and f) of annual streamflow. The performances of seasonal time scale partitioning in approximating annual flow duration curve and estimation of mean and variance of annual streamflow are better than the monthly time scale partitioning. This may be due to the influence of longer duration in seasons which considers intra-seasonal carry over flows during monsoons. At monthly time scale, the carry over flows across different months are not considered in the framework.

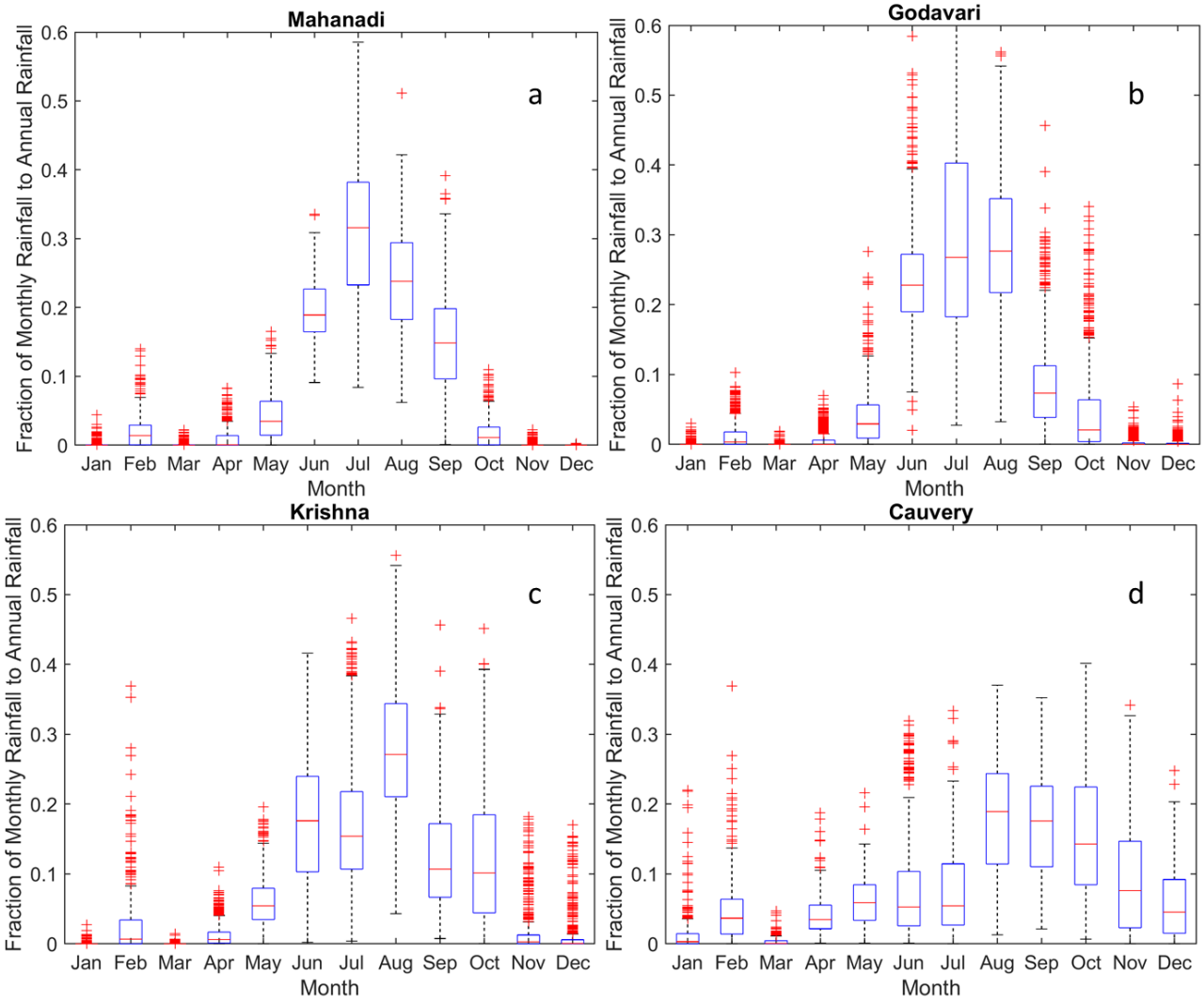


**Figure S6.** Long-term (1951-2010) fractional contribution of monthly rainfall to annual rainfall across Peninsular basins

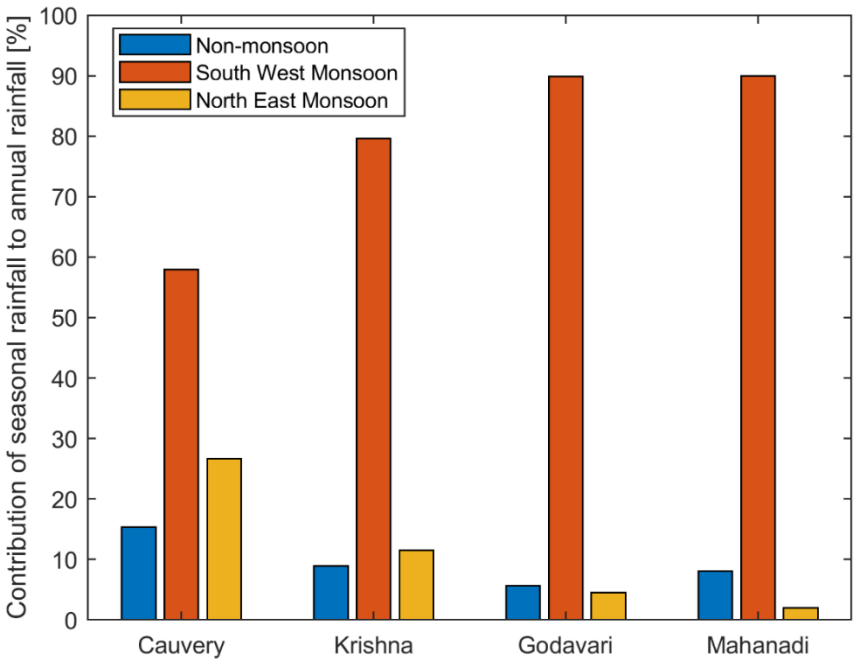


**Figure S7**. Contributions of seasonal rainfall to annual rainfall for long-term (1951-2010) period.

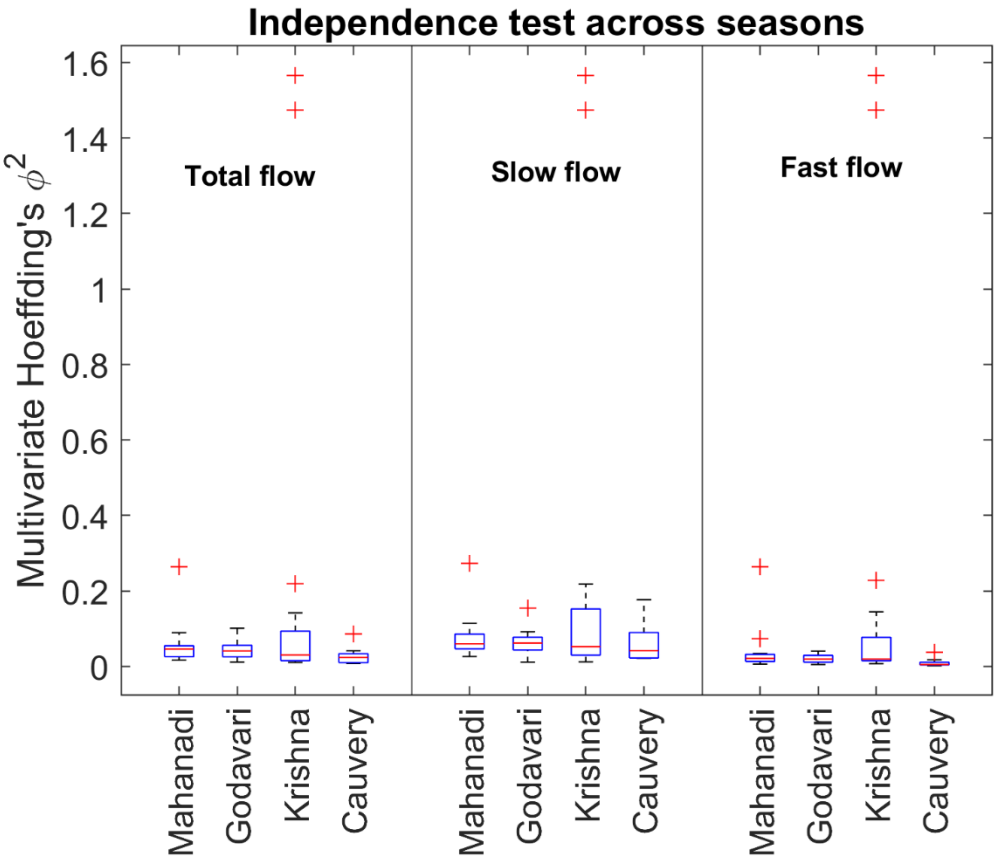


**Figure S8**: Test of independence across seasonal flows.

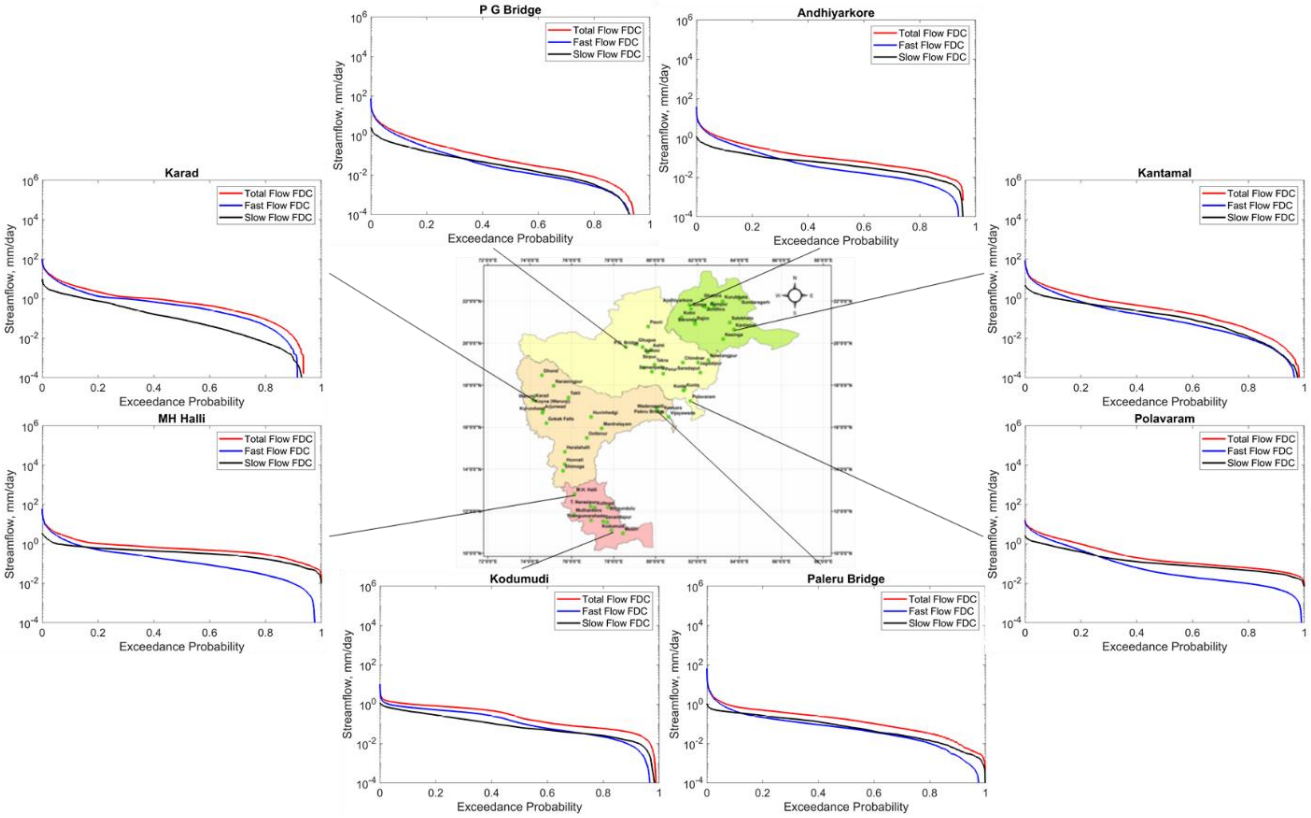


**Figure S9**: Spatial variation of slow, fast and total flow duration curves across Peninsular region. The fast and slow flow duration curves in the northern part of the region cut off after sustaining for 90% of the time. However, in the southern region, slow flow duration curves sustain throughout the entire duration, with magnitude higher than that of fast flow.

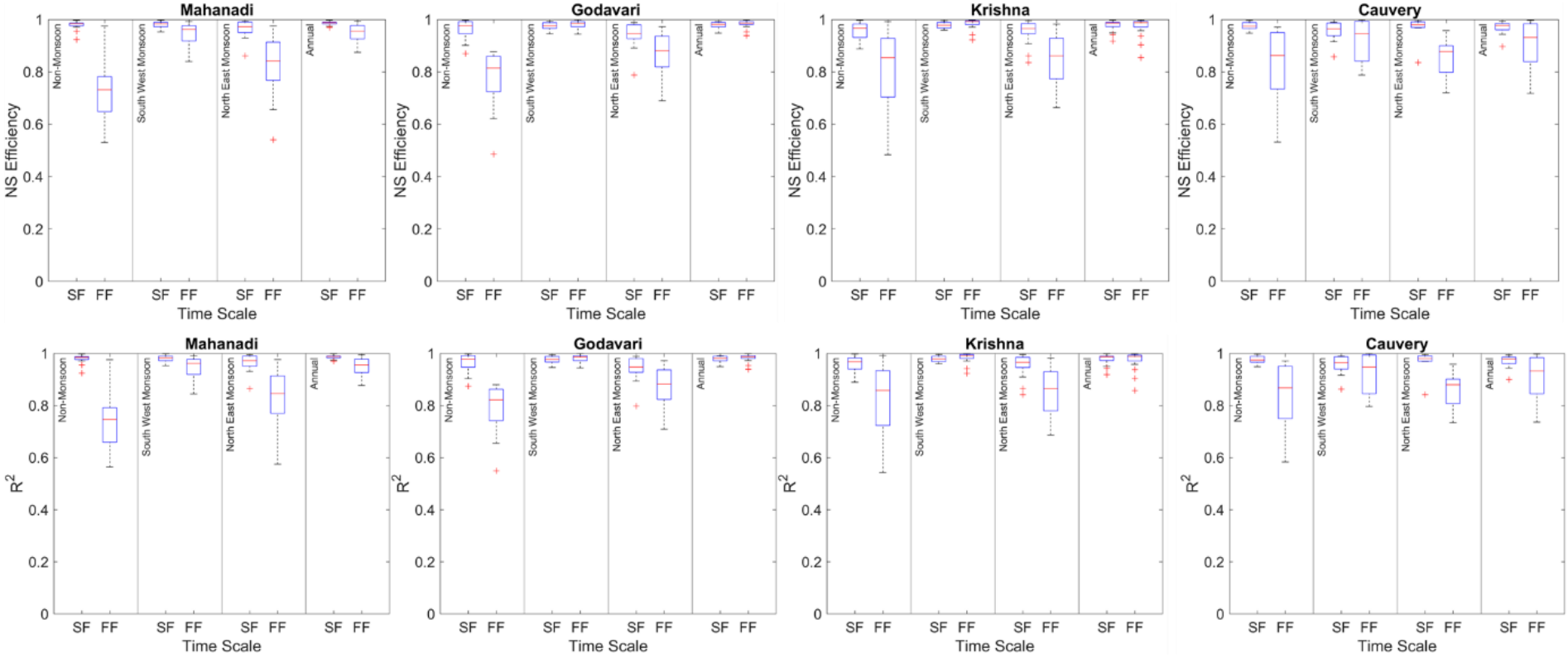


**Figure S10**: Goodness of fit of mixed gamma distribution for fast and slow flow components at seasonal scales. The values of coefficient of determination ($R^2$) and Nash-Sutcliffe efficiency (NSE) represent how well the observed flow duration curve is simulated using mixed gamma distribution model. It is observed that, the magnitude of $R^2$ of slow flow across all seasons is higher than that of fast flow. This is due to the fact that slow flow has higher residence time in the system which tend to reduce the variability in the flow dynamics. The nature of the geologic formations that supports the transmission of slow flow is one of the major factors controlling the slow flow variability. The performance of fast flow ($R^2$) is better during South-West monsoon season – the dominating season for streamflow generation.

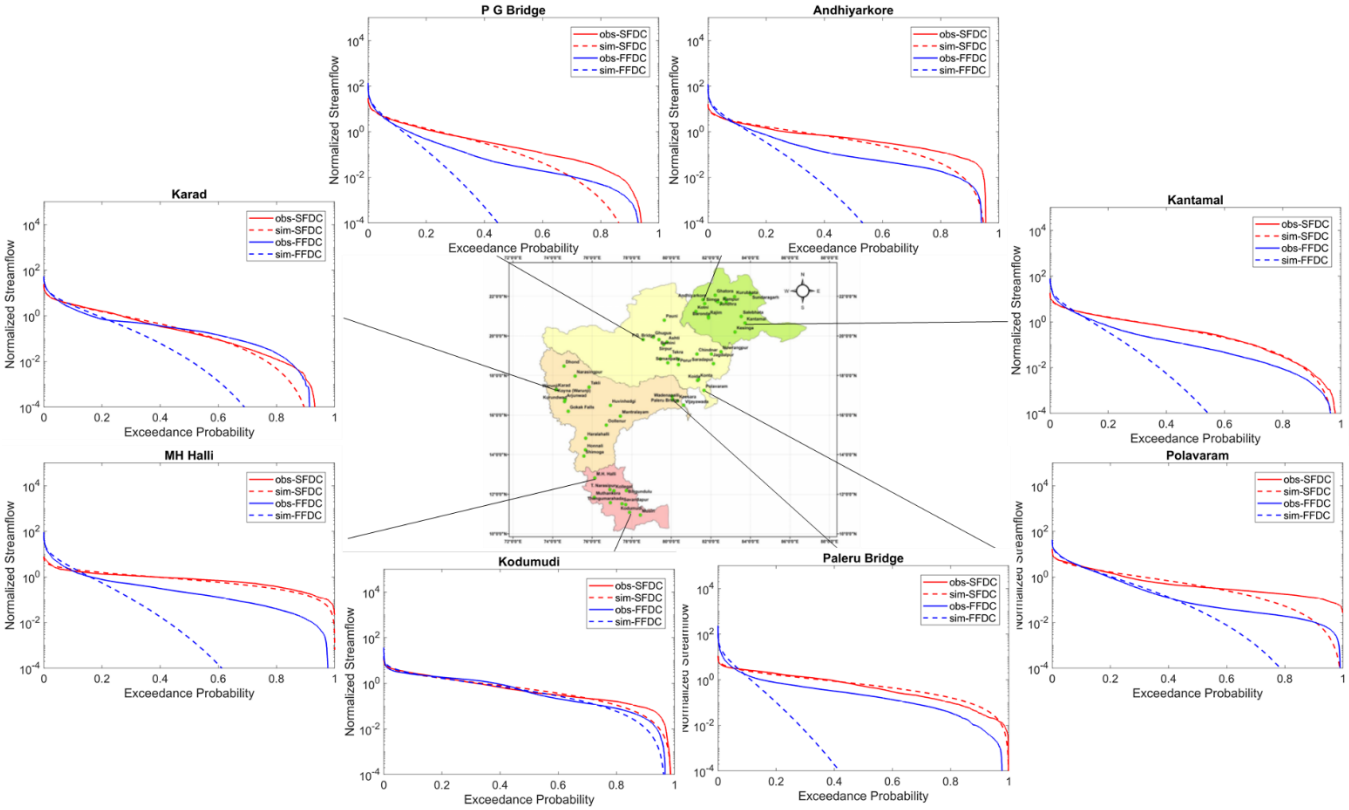


**Figure S11**: Normalized empirical FDCs and mixed gamma distribution fits for slow flow and fast flow. The logarithmic scale in y-axis tend to exaggerate the poor fits.

**S1: Details of the River Basins:**

With an annual average rainfall of 1096 mm, the Godavari, the largest of all Peninsular rivers, receives nearly 84 percent of its annual rainfall on average during the South-West monsoon (Koneti et al., 2018). The Godavari basin's challenges include frequent flooding in its deltaic lower reaches, given the area's proximity to the coastal zone, which is prone to cyclones, and frequent drying up during the drier months (Koneti et al., 2018). Krishna is Peninsular India's second-largest river, with a total catchment area of 2,60,000 $km^2$, and is susceptible to floods and droughts in some specific regions (Chanapathi & Thatikonda, 2020). The Mahanadi basin constitutes a total catchment area of about 141,600 $km^2$ with an average annual rainfall of 1,360 mm and a mean annual river flow of 66,640 million $m^3$ (Rao et al., 2017). The South-West monsoon is the most significant contributor to rainfall in the Krishna basin, accounting for about 90% of its total rainfall; the Krishna Basin, however, has a non-uniform rainfall distribution caused by climate variability, with an average annual rainfall about of 770 mm (Chanapathi & Thatikonda, 2020). Annual rainfall in the Cauvery varies from 621 mm in the lower reaches to 4137 mm in the mountainous uplands, exhibiting considerable variation across the basin (Kumar Raju & Nandagiri, 2017). The river Krishna, with a mean annual runoff of less than 100 mm, is designated as an arid river (Milliman JD, 2011; Gupta et al., 2022), Cauvery as a semiarid river (100-250 mm), Mahanadi and Godavari as humid rivers (250–750 mm). The higher baseflow index occurs within 0.5 and 0.7 in catchments in the Godavari and Mahanadi basins, whereas the lower baseflow index is noted from 0.25 and 0.45 in the Cauvery and Krishna basins (Bhardwaj et al., 2020). For agricultural purposes, the semiarid regions of the Cauvery basin rely more on groundwater than surface water when compared to the other three basins (Sreelash et al., 2020).

**S2: Independence between Flows Across Seasons:**

The multivariate Hoeffding test (Gaißer et al., 2010) is conducted to check the independence between three random variables representing Non-monsoon, Southwest Monsoon and Northeast Monsoon flows respectively. A value of test statistic – $\varphi^2$ – close to zero indicates independence between three random variables. It is observed that except for two stations in Krishna basin, 60 out of 62 stations are showing independence between flows across seasons (Figure S8). Therefore, the assumption of no carry-over is used to construct annual FDC based on seasonal FDCs.

**S3: Supporting Equations on Time Scale Partitioning:**

If $F_A(.)$, $F_{NM}(.)$, $F_{SW}(.)$ and $F_{NE}(.)$ represent cumulative distribution function of daily flows during annual, Non-monsoon, South-West monsoon and North-East monsoon, respectively, then using equation (2), equation (6) can be written as:

$$1 - F_A(q) = \tau_1[1 - F_{NM}(q)] + \tau_2[1 - F_{SW}(q)] + \tau_3[1 - F_{NE}(q)] \quad \text{(S1)}$$

Differentiating the above equation with respect to $q$ ,

$$f_A(q) = \tau_1 f_{NM}(q) + \tau_2 f_{SW}(q) + \tau_3 f_{NE}(q) \quad \text{(S2)}$$

where $f_A(.)$, $f_{NM}(.)$, $f_{SW}(.)$ and $f_{NE}(.)$ represent probability density functions of annual, Non-monsoon, South-West monsoon and North-East monsoon flows respectively.

If $Q$, $Q_{NM}$, $Q_{SW}$ and $Q_{NE}$ represent random variables comprising of daily streamflow at annual, Non-monsoon, South-West monsoon and North-East monsoon time scales respectively, the expectation $E(Q)$ and variance $V(Q)$ of annual flow in terms of seasonal flows can be expressed as

$$E(Q) = \tau_1 E(Q_{NM}) + \tau_2 E(Q_{SW}) + \tau_3 E(Q_{NE}) \quad \text{(S3)}$$

$$V(Q) = \tau_1 E(Q_{NM}^2) + \tau_2 E(Q_{SW}^2) + \tau_3 E(Q_{NE}^2) - \big(E(Q)\big)^2 \quad \text{(S4)}$$

The magnitudes of $\tau_1$, $\tau_2$ and $\tau_3$ are $\frac{5}{12}, \frac{4}{12}$ $and$ $\frac{3}{12}$ based on the annual proportions of Non-monsoon, South-West monsoon and North-East monsoon respectively.

The same concept can be continued by combining the flows in different months, in which case the way to combine monthly FDCs into an annual FDC is given by:

$$\mathrm{D(q)} = \frac{1}{12}\sum_{m=1}^{12} \mathrm{D_m(q)} \quad \text{(S5)}$$

where $m = 1, \ldots, 12$.

If $Q_m$ represents the random variable daily streamflow over $\mathrm{m^{th}}$ month, then the expectation $E(Q)$ and variance $V(Q)$ of annual flow in terms of monthly flows can be expressed as

$$E(Q) = \frac{1}{12}\sum_{m=1}^{12} E(Q_m) \tag{S6}$$

$$V(Q) = \frac{1}{12}\sum_{m=1}^{12} E(Q_m^2) - \left(E(Q_A)\right)^2 \tag{S7}$$

**S4: Fitting statistical distributions:**

A simple statistical distribution, the mixed gamma distribution, is employed here to characterize the FDC in Peninsular River system. The choice of the mixed gamma distribution is made to take care of the flow regimes of the selected basins (i.e., to accommodate the presence of zero flow values) (Cheng et al., 2012). The classic gamma distribution is a two-parameter, continuous distribution with a shape parameter, *k*, and a scale parameter, $\theta$. In addition, the probability of zero flows, α, is defined as the ratio of the number of zero flow days to the total number of days within the data record. The mixed gamma distribution (Cheng et al., 2012) employed to model FDC is as follows:

$$f\ (q,k,\theta,\alpha) = \begin{cases} \alpha, & q\ = 0 \\ (1-\alpha).\, g(q,k,\theta), & q\ > 0 \end{cases} \tag{S8}$$

where $g(q,k,\theta)$ is the probability density function of the gamma distribution. The probability density function of the gamma distribution is assumed to take the form of (Cheng et al., 2012):

$$g\ (q,k,\theta) = \frac{1}{|\theta|\,\Gamma\,(k)} \left(\frac{q}{\theta}\right)^{k-1} \exp\left(-\frac{q}{\theta}\right) \tag{S9}$$

where $k$ and $\theta$ are the shape and scale parameters, respectively. The parameters $k$ and $\theta$ can be estimated by the method of moments. The mean, μ, and variance, ν, of the gamma distribution are evaluated from the $q\ > 0$ time series. The parameters are related to μ and $\nu$ as follows:

$$\mu = \ k\,.\,\theta \tag{S10}$$

$$\nu = k\,.\,\theta^2 \tag{S11}$$

The following formulation is used to obtain the flow given a probability of exceedance, $p$ (Cheng et al., 2012):

$$q\ (p,k,\theta,\alpha) = \begin{cases} G^{-1}\left(1 - \frac{p}{1-\alpha}, k, \theta\right), & 0 \le p\ \le 1-\alpha \\ 0 \qquad\qquad\qquad\quad , & 1-\alpha\ < p\ \le 1 \end{cases} \tag{S12}$$

where $G^{-1}$ is the inverse of the CDF of the mixed gamma distribution.

In this case, given that we have already looked at the climatic and landscape controls on the mean annual flows, we instead work with the normalized daily streamflow time series (i.e., daily streamflow divided

by long-term mean daily streamflow), which is then used to estimate the parameters of the mixed gamma distribution. The parameters estimated from the normalized streamflow series can thus be used to infer secondary controls on the shape of flow duration curves.

**S5: Baseflow decomposition (Recursive Digital Filter):**

The partitioning of total flow ($Q$) into slow flow ($Q_s$) is performed using recursive digital filter technique as described in Arnold & Allen (1999) and Arnold et al. (1995). Based on the study by Nathan and McMahon (1990), they found that a coefficient range between 0.9 and 0.95 yielded most acceptable baseflow separation. Therefore, we have taken the value 0.95 as a coefficient value for this analysis (more discussion is provided at the end of T5). This filter is applied to daily streamflow timeseries data for all the gauging stations across the Peninsular region.

The equation of the filter is

$$q_t = \varepsilon q_{t-1} + \frac{(1+\varepsilon)}{2}(Q_t - Q_{t-1}) \quad \text{(S13)}$$

where $q_t$ is the filtered surface runoff (quick response) at the $t$ time step, $Q$ is the original streamflow (total flow), and ε is the filter parameter (which is assumed to be 0.95). Slow flow, $Q_s$, is calculated with the equation:

$$Q_s = Q - q_t \quad \text{(S14)}$$

After obtaining the slow flow component, the fast flow ($Q_f$) is obtained by subtracting $Q_s$ from $Q$.

$$Q_f = Q - Q_s \quad \text{(S15)}$$

In order to demystify the role of different values of the filter parameter in the digital recursive filter, the model was run for three different seasons for all the catchments in Peninsular region. The results are presented in Figure S12.

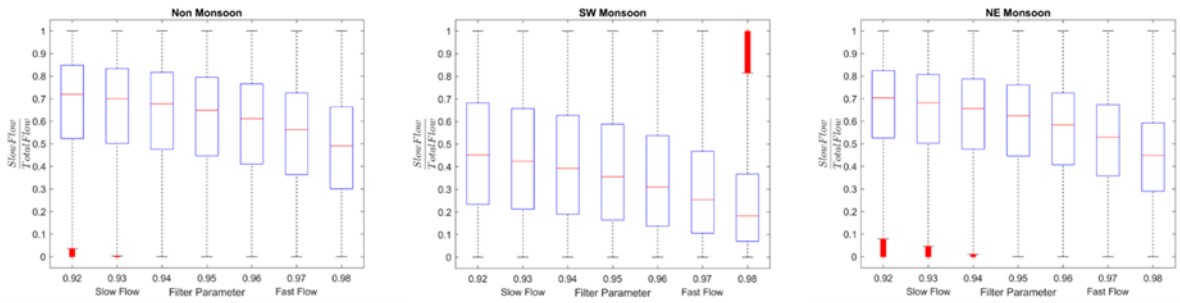


**Figure S12.** Contribution of slow flow to total flow for different seasons. The box plots in each season represent the partitioning of total flow into slow flow for different filter parameters, viz. [0.92,0.93,0.94,0.95,0.96,0.97 ,0.98].

It is observed that the median variations in the slow flow fraction during non-monsoon period (0.5-0.7), south west monsoon period (0.18-0.45) and north east monsoon period (0.44-0.7) which lies within

30% variation. However, even with these variations, the overall pattern, i.e., high slow flow contribution during non-monsoon and north east monsoon seasons and low slow flow contribution during south west monsoon remains intact, revealing seasonal changes in the dynamics of slow flow contribution to total flow. In this paper, we assumed the parameter 0.95 reflecting the average variability in slow flow contributions to total flow.

**S6: Recession Analysis:**

In recession analysis, it is often assumed that rate of change of streamflow $\frac{dQ}{dt}$ and streamflow $(Q)$ follows a power law in the form:

$$-\frac{dQ}{dt} = \gamma Q^{\beta} \quad \text{(S16)}$$

The parameter $\gamma$ is function of static watershed properties (i.e., hydrological conductivity, drainable porosity, aquifer depth, aquifer breadth, impermeable layer slope and length of stream) (Tashie et al., 2020a). The parameter $\beta$ represents the geometry of the contributing aquifer and water table elevation profile that defines the early and late periods of recession (Tashie et al., 2020b). $\frac{dQ}{dt}$ is estimated using exponential time stepping scheme (Roques et al., 2017). Strictly decreasing recession segments ($\frac{dQ}{dt} < 0$) with recession segments more than 5 days are considered for the estimation of the parameters ($\gamma \; and \; \beta$) (Jachens et al., 2020). A weighted least square regression is used to fit a line in log-log space to recession segments (Roques et al., 2017). The median of the parameters is used to describe catchment-average recession behaviour (Gnann et al., 2021).

**S7: Absolute contributions of fast and slow flow to total flow:**

The absolute contributions of fast and slow flow to total flow are determined using the coefficient of determination ($R^2$) of simple linear regression models, that measures the reduction in variability of total flow due to fast and slow flow components. The details are given below:

Model 1: $Q = \varphi_1 \cdot Q_f + \epsilon_1$ (S17)

Model 2: $Q = \varphi_2 \cdot Q_s + \epsilon_2$ (S18)

The coefficient of determination measures the effect of slow(fast) flow in reducing the variation in total flow based on Model1(Model2). Higher the value of this coefficient, higher the contribution of slow/fast flow in reducing the variation in total flow.

The coefficient of determinations for two models can be estimated as:

$$R^2_{(1)} = \frac{SSR^{(1)}}{SSTO} \quad \text{(S19)}$$

$$R^2_{(2)} = \frac{SSR^{(2)}}{SSTO} \quad \text{(S20)}$$

where, $SSR^{(1)}$ and $SSR^{(2)}$ represent the regression sum of squares for Model 1 and Model 2 respectively, and SSTO represents the total sum of squared deviations from mean, i.e., $SSTO = \sum(Q_i - \bar{Q})^2$. The sum of squares due to the models are expressed as:

$SSR^{(1)} = \sum\left(\widehat{Q_{(1)}} - \bar{Q}\right)^2$ and $SSR^{(2)} = \sum\left(\widehat{Q_{(2)}} - \bar{Q}\right)^2$ where $\widehat{Q_{(1)}}$ *and* $\widehat{Q_{(2)}}$ are the fitted values of total flow using Model 1 and Model 2 respectively.

The values of coefficient of determination ($R^2$) for three seasons are shown in Fig. S13.

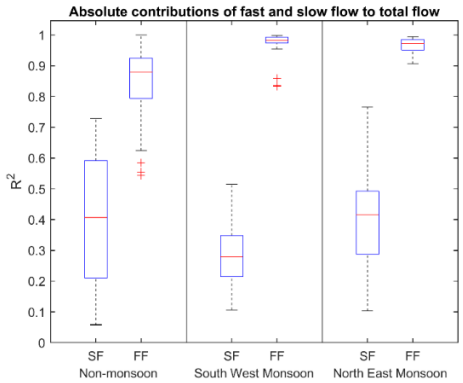


**Figure S13.** Coefficient of determination representing the absolute contribution of fast/slow flow in reducing the variation in total flow across seasons.

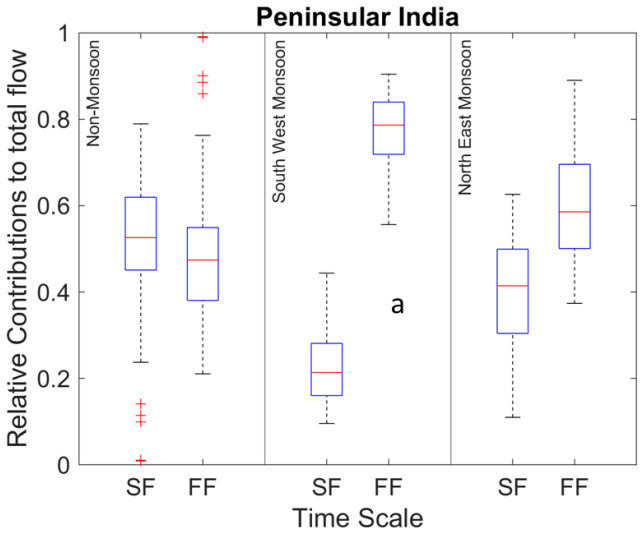


**Figure S14.** Relative contributions of fast (FF) and slow flow (SF) to total flow at regional and seasonal scales (NM – Non-monsoon, SW – South-West monsoon and NE – North-East monsoon).

It can be shown that the pattern of absolute contribution remains similar (in terms of phase relationship between slow and fast flow contributions to total flow) with that of relative contribution as reported in Fig S13. However, there are differences in the magnitudes of the absolute contributions and relative contributions (Fig. S14) of the flow components to total flow. The major difference between relative and absolute contribution analyses is that the contribution of the fast flow is significantly higher than the slow flow for non-monsoon season, which can be attributed to rainfall during the non-monsoon period (Fig S6).

**S8: Investigating the slow flow fraction of total flow in Peninsular India:**

The variability in slow flow fraction (SFF) is investigated using multiple linear regression by considering the recession parameters, $\beta$ and $\gamma$ in the equation $-\frac{dQ}{dt} = \gamma Q^{\beta}$ and the location of the gauge (δ, latitude). The results are provided below:

*Regression Model:*

$$SFF = \alpha_0 + \alpha_1\gamma + \alpha_2\beta + \alpha_3\delta \quad \text{(S21)}$$

**Table S1** – Statistical Assessment of regression coefficients

| Coefficients | Estimate | SE | tStat | pValue |
|---|---|---|---|---|
| $\alpha_0$, (Intercept) | 0.35361 | 0.055275 | 6.3973 | 2.99E-08 |
| $\alpha_1$ | -0.024117 | 0.021119 | -1.142 | 0.25816 |
| $\alpha_2$ | 0.12791 | 0.025704 | 4.9764 | 6.12E-06 |
| $\alpha_3$ | -0.015556 | 0.0023978 | -6.4875 | 2.12E-08 |

The above regression model was able to explain to about 52% of the variability in slow flow fraction of total flow (p-value = $1.98 \times 10^{-9}$), and in general, the model is found to be useful to explain SFF in terms of recession parameter and latitude. A fraction of the unexplainable part in SFF can be attributed to the heterogeneity in subsurface geologic formations and dam induced variations in the catchment storages. However, at a regional scale, the south-north gradient (represented by the parameter $\delta$) can explain the variability in slow flow fraction to total flow. This regional setting is an important outcome to understand the streamflow variability in Peninsular region of India.

## References


1. Arnold, J. G. and Allen, P. M.: Automated methods for estimating baseflow and ground water recharge from streamflow records, J. Am. Water Resour. Assoc., 35, 411–424, https://doi.org/10.1111/j.1752-1688.1999.tb03599.x, 1999.
2. Arnold, J. G., Allen, P. M., Muttiah, R., and Bernhardt, G.: Automated Base Flow Separation and Recession Analysis Techniques, Ground Water, 33, 1010–1018, https://doi.org/10.1111/j.1745-6584.1995.tb00046.x, 1995.
3. Bhardwaj, K., Shah, D., Aadhar, S., and Mishra, V.: Propagation of Meteorological to Hydrological Droughts in India, J. Geophys. Res. Atmos., 125, https://doi.org/10.1029/2020JD033455, 2020.
4. Chanapathi, T. and Thatikonda, S.: Investigating the impact of climate and land-use land cover changes on hydrological predictions over the Krishna river basin under present and future scenarios, Sci. Total Environ., 721, 137736, https://doi.org/10.1016/j.scitotenv.2020.137736, 2020.
5. Cheng, L., Yaeger, M., Viglione, A., Coopersmith, E., Ye, S., and Sivapalan, M.: Exploring the physical controls of regional patterns of flow duration curves – Part 1: Insights from statistical analyses, Hydrol. Earth Syst. Sci., 16, 4435–4446, https://doi.org/10.5194/hess-16-4435-2012, 2012
6. Gaißer, S., Ruppert, M., & Schmid, F. (2010). A multivariate version of Hoeffding's Phi-Square. Journal of Multivariate Analysis, 101(10), 2571 2586.https://doi.org/10.1016/j.jmva.2010.07.006
7. Gupta, H., Reddy, K. K., Gandla, V., Paridula, L., Chiluka, M., and Vashisth, B.: Freshwater discharge from the large and coastal peninsular rivers of India: A reassessment for sustainable water management, Environ. Sci. Pollut. Res., 29, 14400–14417, https://doi.org/10.1007/s11356-021-16811-0, 2022.
8. Jayaraman, A., Venkat Ratnam, M., Patra, A. K., Narayana Rao, T., Sridharan, S., Rajeevan, M., Gadhavi, H., Kesarkar, A. P., Srinivasulu, P. & Raghunath, K. (2010). Study of atmospheric forcing and responses (SAFAR) campaign : Overview. Annales Geophysicae. January 2010. https://doi.org/10.5194/angeo-28-89-2010.
9. Koneti, S., Sunkara, S. L., and Roy, P. S.: Hydrological modeling with respect to impact of land-use and land-cover change on the runoff dynamics in Godavari river basin using the HEC-HMS model, ISPRS Int. J. Geo-Information, 7, https://doi.org/10.3390/ijgi7060206, 2018.
10. Krishnamurthy, V., & Ajayamohan, R. S. (2010). Composite Structure of Monsoon Low Pressure Systems and Its Relation to Indian Rainfall. Journal of Climate, 23(16), 4285–4305. https://doi.org/10.1175/2010JCLI2953.1
11. Kumar Raju, B. C. and Nandagiri, L.: Analysis of historical trends in hydrometeorological variables in the upper Cauvery Basin, Karnataka, India, Curr. Sci., 112, 577–587, https://doi.org/10.18520/cs/v112/i03/577-587, 2017.
12. Milliman JD, F. K.: River discharge to the coastal ocean: a global synthesis, river discharge to the coastal ocean: a global synthesis, Cambridge University Press, 2011.
13. Nathan, R. J. and McMahon, T. A.: Evaluation of automated techniques for base flow and recession analyses, Water Resour. Res., 26, 1465–1473, https://doi.org/10.1029/WR026i007p01465, 1990.
14. Prakash, S., Mitra, A. K., & Pai, D. S. (2015). Comparing two high-resolution gauge-adjusted multisatellite rainfall products over India for the southwest monsoon period. Meteorological Applications, 22(3), 679–688. https://doi.org/10.1002/met.1502
15. Rao, P. G., Chanapathi, T., Thatikonda, S., Koneti, S., Sunkara, S. L., Roy, P. S., Kumar Raju, B. C., and Nandagiri, L.: Investigating the impact of climate and land-use land cover changes on hydrological predictions over the Krishna river basin under present and future scenarios, Curr. Sci., 7, 577–587, https://doi.org/10.18520/cs/v112/i03/577-587, 2017.
16. Roques, C., Rupp, D. E., & Selker, J. S. (2017). Improved streamflow recession parameter estimation with attention to calculation of -dQ/dt. Adv. in Wat. Resour., 108, 29–43. https://doi.org/10.1016/j.advwatres.2017.07.013
17. Sreelash, K., Mathew, M. M., Nisha, N., Arulbalaji, P., Bindu, A. G., and Sharma, R. K.: Changes in the hydrological characteristics of Cauvery river draining the eastern side of southern Western Ghats, India, Int. J. River Basin Manag., 18, 153–166, https://doi.org/10.1080/15715124.2020.1719119, 2020.